NRL Report 7398

Gl

Theoretical and Experimental Impact Studies

[Unclassified Title]

W. E. JOHNSON

Systems Science and Software
La Jolla, California

AND

S. T. ZALESAK

Hypervelocity Techniques Branch
Plasma Physics Division

November 3, 1972

APPROVED FOR PUBLIC
RELEASE - DISTRIBUTION
UNLIMITED

NAVAL RESEARCH LABORATORY
Washington, D.C.

CONTENTS

Abstract ii
Problem Status ii
Authorization ii

INTRODUCTION 1

THE HYDRODYNAMICS AND STRENGTH FORMULATION FOR THE DORF CODE 1

THE EQUATION-OF-STATE MODEL USED IN THE DORF AND DORF9 CODES 2

COMPARISON BETWEEN CALCULATIONS AND EXPERIMENTS 3

Shock Propagation into Semi-Infinite Targets for Like and Unlike Material Hypervelocity Impacts (DORF and DORF9) 3
Single-Plate Rod Impact Calculations (DORF) 15
Low-Velocity Multimaterial Impact (DORF9) 15

CONCLUSIONS 23

REFERENCES 23

APPENDIX A — Simplified Flow Chart for DORF9 24

ABSTRACT
[Unclassified]

Thin, layered, and semi-infinite targets have been subjected to high velocity projectile impacts experimentally, and theoretical calculations performed by the DORF code for these same target impacts. The DORF code is a two-material, two-dimensional continuous Eulerian hydrodynamic code coupled with a rigid, perfectly plastic strength model. In addition, DORF9, a nine-material version of DORF, has calculated several of the impact experiments. The agreement is good between the theoretical calculations and experimental values for shock attenuation and projectile length loss.

PROBLEM STATUS

This is a final report on this phase of the project; work is continuing on other phases.

AUTHORIZATION

NRL Problem F04-21
ARPA Order 854, Program Code 8E20
Project N00014-70-C-0002

Manuscript submitted February 1, 1972.

THEORETICAL AND EXPERIMENTAL IMPACT STUDIES
[Unclassified Title]

INTRODUCTION

Significant improvements have been made in the strength and transport formulation of the DORF code (1). In addition, the code has been modified to allow the treatment of up to nine different equations of state in the same problem (2).

It was felt that at some point experiments should be performed to substantiate the results from the code calculations. As a result, several impacts into thin, layered, and semi-infinite targets have been performed experimentally at NRL. Shock-propagation, shock-attenuation, and projectile-loss comparisons between theory and experiment have shown very good agreement.

As a result, we feel confident that numerical techniques, such as the DORF code, can be applied to a variety of interesting problems with a high degree of success.

THE HYDRODYNAMICS AND STRENGTH FORMULATION FOR THE DORF CODE

The DORF and DORF9 codes numerically solve the Eulerian equations of hydrodynamic flow, which are basically statements of mass, momentum, and energy conservation respectively:

$$\frac{\partial \rho}{\partial t} + \nabla \cdot (\rho \mathbf{u}) = 0$$

$$\frac{\partial \rho \mathbf{u}}{\partial t} + \nabla \cdot (\rho \mathbf{u}\mathbf{u}) = -\nabla P$$

$$\frac{\partial \rho E}{\partial t} + \nabla \cdot (\rho E \mathbf{u}) = -\nabla \cdot (P \mathbf{u}),$$

where

$\mathbf{u}$ = flux vector

ρ = material density

P = hydrostatic pressure

E = specific internal energy.

As a separate step, the momentum and energy conservation equations for material strength are solved:

$$\rho \frac{\partial u_i}{\partial t} = \sigma_{ij,j}$$

$$\rho \frac{\partial E}{\partial t} = (\sigma_{ij} u_i)_{,j},$$

where σ_{ij} is the stress deviation tensor and the summation and implied differentiation conventions apply. An elementary flow chart showing the manner and order in which DORF and DORF9 solve these equations is given in Appendix A. Reference 1 gives a more complete description of the methodology.

THE EQUATION-OF-STATE MODEL USED IN THE DORF AND DORF9 CODES

The equation of state used in the DORF and DORF9 codes is given in a report by Tillotson (3); it yields pressure P as a function of volume V and specific internal energy E. For condensed states, when $\rho/\rho_0 > 1$ or for any cold state when $E < E_s$, the equation becomes

$$P = P_C = E\rho\left(a + \frac{b}{E/E_0\eta^2 + 1}\right) + A\mu + B\mu^2,$$

where

ρ_0 = initial (zero pressure) density of material

E_s = energy required to bring material to vaporization point

$$\eta = \rho/\rho_0$$

$$\mu = \eta - 1$$

and a, b, A, B, and E_0 are empirical fits to the experimental data. A cutoff is built into the codes which does not allow the use of $\mu < -A/2B$ in this equation since this could allow $\partial P/\partial V$ to be positive.

For expanded states, where $\rho/\rho_0 < 1$ and $E > E_s'$, the equation of state is

$$P = P_E = aE\rho + \left\{\frac{bE\rho}{(E/E_0\eta^2) + 1} + A\mu e^{-\alpha[(\rho_0/\rho) - 1]}\right\} e^{-\beta[(\rho_0/\rho) - 1]^2},$$

where $E_s' = E_s$ plus the energy of vaporization, and α and β are empirical constants.

In the intermediate region, where $\eta < 1$ and $E_s < E < E_s'$, a smooth transition between the condensed and expanded states is assured by setting

$$P = \frac{P_E(E - E_s) + P_C(E_s' - E)}{E_s' - E_s}.$$

When the term $E/E_0\eta^2 \ll 1$, the equation for P_C behaves like a Mie-Gruneisen equation of state with a constant Gruneisen ratio of $a + b$. At large energies and moderate compressions, $E/E_0\eta^2 \gg b$ and μ small, P_C behaves like a gaseous equation of state:

$$P = a\rho E.$$

The Gruneisen ratio over all energy and densities for which P is valid is given by

$$G(E, \rho) \equiv V\left(\frac{\partial P}{\partial E}\right)_V = a + \frac{b}{(E/E_0\eta^2) + 1}.$$

The yield strength is represented by

$$Y = (Y_0 + \alpha' P)\left(1 - \frac{E}{E_m}\right),$$

where α' is approximately 0.07 for metals and E_m is the energy required to melt the material. If E is greater than E_m, Y is set to zero.

The stress deviators are defined as

$$\sigma_{ij} = B\dot{\epsilon}_{ij},$$

where

$$B = \frac{Y\sqrt{2}}{\sqrt{\dot{\epsilon}_{ij}\,\dot{\epsilon}_{ij}}}$$

σ_{ij} = stress deviation tensor

$\dot{\epsilon}_{ij}$ = strain rate deviation tensor

and the summation convention again applies.

COMPARISON BETWEEN CALCULATIONS AND EXPERIMENTS

Shock Propagation into Semi-Infinite Targets for Like and Unlike Material Hypervelocity Impacts (DORF and DORF9)

Two shock propagation experiments, hereafter referred to as shot 1 and shot 2, were performed, and the corresponding code calculations completed using DORF and DORF9.

Shot 1

A 3/8-in.-diameter aluminum sphere was impacted normally into a semi-infinite 1100F aluminum target at 7.091 km/sec. The decay of the on-axis peak pressure of the shock wave was observed using manganin pressure gauges imbedded at various points within the aluminum target (4). Additional experimental data was obtained from the work of Charest (5), who obtained peak pressures using free-surface particle velocity techniques. Both sets of data are shown in Fig. 1. The DORF code was then used to calculate this same impact, and the calculated pressures were compared with the

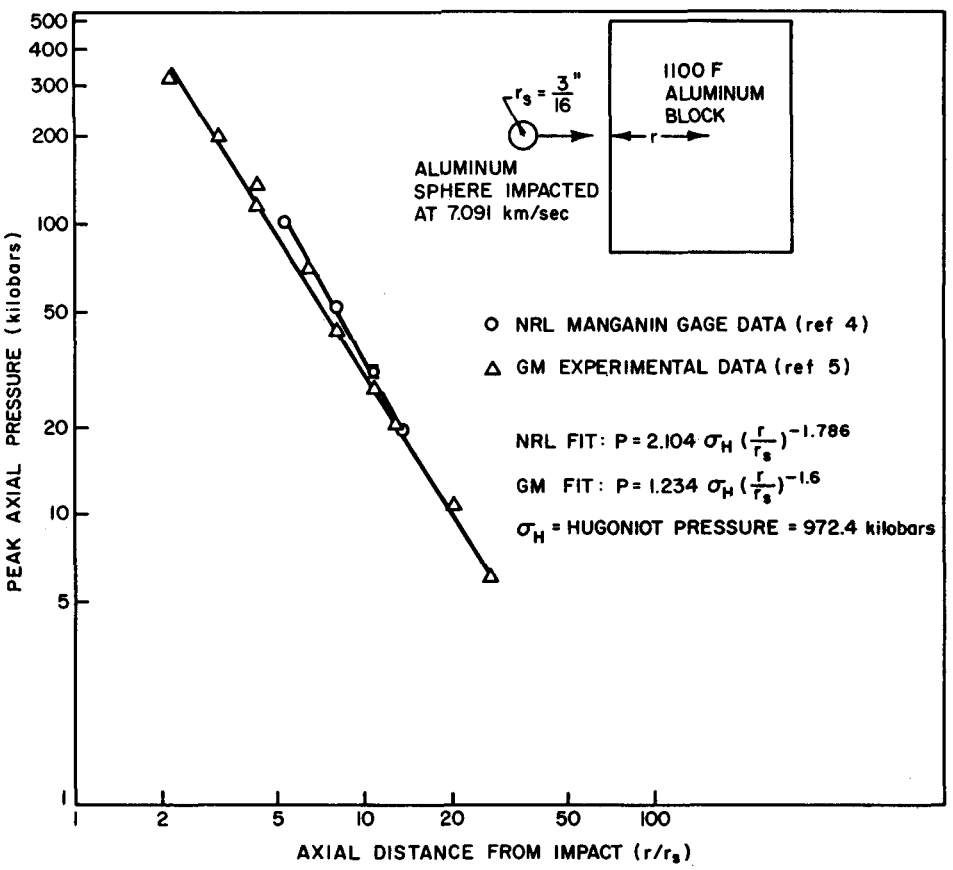

Fig. 1 — Configuration and experimental data for shot 1

experimental values. The results were somewhat disappointing at first because the DORF code values were consistently lower than either of the experimental measurements, although there was a convergence in the lower pressure regions (large distances from the impact point). Reasons for the discrepancy were difficult to find, and suspicion finally settled on the Tillotson equation of state for aluminum.

A plot of shock velocity U_s versus particle velocity U_p was derived from the Tillotson formulation, and the results were compared with the experimental data of Rice, McQueen, and Walsh (6) and of Al'tshuler et al (7). As shown in Fig. 2, the Tillotson equation starts deviating from the experimental values fairly quickly, reaching a value for U_s that is about 8% low at the Hugoniot conditions for shot 1 ($U_p \approx 3.5$ km/sec.). This means that the Tillotson equation of state would predict a Hugoniot pressure that is 8% low for shot 1. This, combined with the generally more compressible (than reality) nature of the Tillotson formulation over the whole range of compression, could conceivably affect both the magnitude and decay rate of the calculated shock wave. To determine whether or not this reasoning applied, a simple Mie-Gruneisen equation-of-state option, using the Hugoniot as the reference pressure curve, was inserted into DORF. The equation of state used the following standard equations:

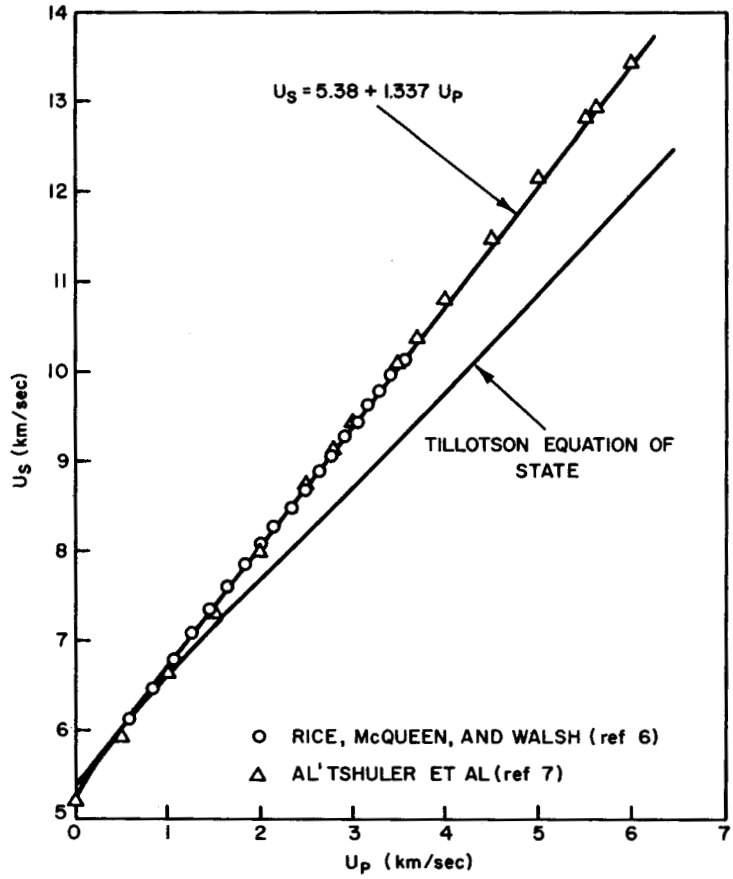

Fig. 2 — Aluminum Hugoniot-experimental data vs Tillotson equation of state

$$P = P_H + G\rho(E - E_H)$$

and

$$P_H = \frac{\rho_0 C_0 W}{(1 - AW)^2},$$

where

$$E_H = (1/2)P_H(V_0 - V)$$
$$W = 1 - (\rho_0/\rho)$$
$$\rho_0 = 2.71 \text{ g/cc}$$
$$G = 2.13$$
$$C_0 = 5.38 \text{ km/sec}$$
$$A = 1.337.$$

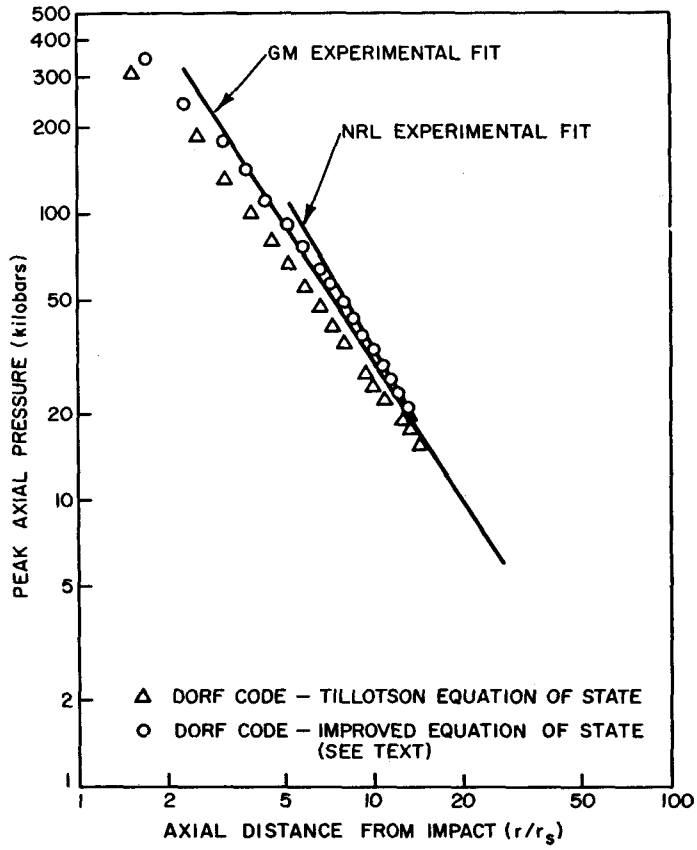

Fig. 3 — DORF code calculations vs experimental data for shot 1

The last two constants come from

$$U_s = C_0 + AU_p$$

and fit the experimental data quite well as can be seen in Fig. 2.

Since our impact is basically a shock propagation problem, the material values near the region of interest should deviate very little from the Hugoniot values. Hence, this equation of state should give highly accurate results.

Shot 1 was then run on DORF using this refined equation of state, and the results again were compared to the experimental values. This time the code gave very satisfying results in terms of their deviation from experimental parts. Both DORF calculations are compared to both experimental determinations in Fig. 3. Axial pressure plots for selected times after impact are shown in Fig. 4. These pressure plots, as well as all others that follow in this report, are derived by assuming that the pressure in a cell represents the pressure at the geometric center of that cell. Peak shock wave pressure is taken to be the largest cell pressure in a given region of interest, and the shock front position to be the geometric center of that cell.

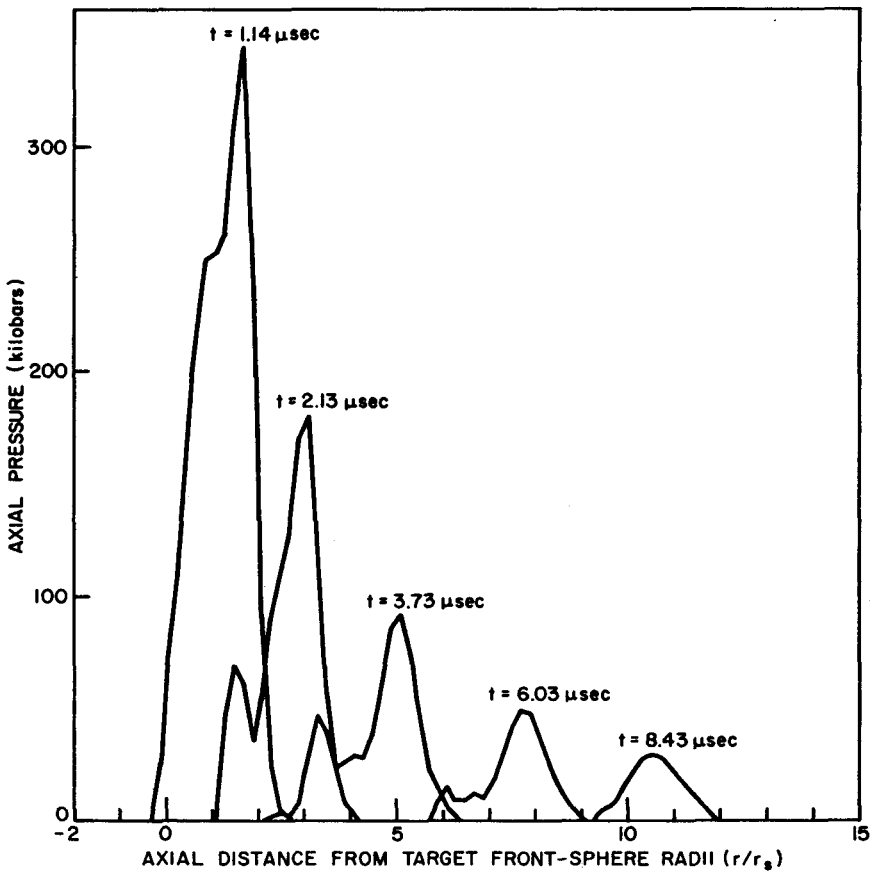

Fig. 4 — Axial pressure plots for shot 1 for selected times after impact

It is clear that shock propagation calculations are extremely sensitive to the equation of state used and that great care should be exercised in selecting an equation of state for such calculations. An unquestioned use of the Tillotson formulation would probably have resulted in the conclusion that Eulerian codes are not particularly suited for the calculation of shock wave propagation problems. It should be pointed out, however, that the Tillotson aluminum equation of state is meant to be used over a much wider range of material conditions than was necessary for this calculation. Also, its unsatisfactory performance for this particular calculation does not necessarily invalidate its use in other calculations. The Tillotson equation of state is probably quite satisfactory for hypervelocity impact calculations where the primary interest lies in the computation of projectile or target deformation. It applies in these cases because most of the physical processes involved occur at pressures much lower than the Hugoniot pressure, where the Tillotson form deviates very little from experimentally observed values.

Shot 2

A 1.27-cm-diameter steel sphere was impacted normally into a 2.5-cm layer of lithium hydride, backed by a 4.5-cm layer of Composition B high explosive, at 5.5 km/sec. The primary interest was in the peak pressure and pulse shape of the shock wave just after it entered the Composition B. Experimentally there were two sources of information:

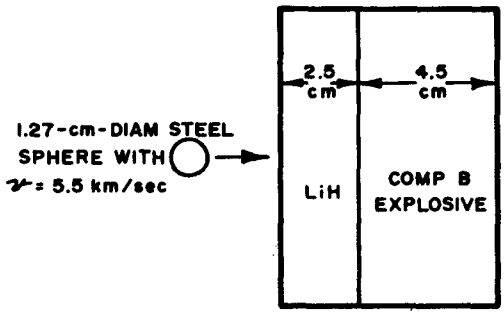

Fig. 5 — Configuration for shot 2

Table 1
Pressure Results for Shot 2

Method of Pressure Measurement	Pressure Entering Composition B (kilobars)
Shock velocity in Composition B	70
Run distance in Composition B	67
DORF9 calculation	70

(a) measurement of the shock velocity just inside the Composition B yielded a peak pressure of 70 kilobars and (b) measurement of the run distance to detonation in the Composition B yielded a peak pressure of 67 kilobars, assuming a pulse width of 0.5 μsec or more. The DORF9 calculation yielded a peak pressure of 70 kilobars and a pulse width of about 1 μsec. (In the DORF9 calculation, the Composition B was treated as an inert substance. No attempt was made to numerically simulate the detonation process.) The shot configuration is shown in Fig. 5, and results are given in Table 1. Shock pressure profiles on axis are shown for various times after impact in Figs. 6 through 9. Again, the agreement between calculated and experimental results is quite satisfactory.

Additional Calculations

In addition to the above, two other similar calculations were performed without experimental counterparts and are referred to as shot 2A and shot 3. The shot configurations are shown in Fig. 10. As can be easily seen, shot 2A has the same configuration as shot 2 but with the Composition B replaced by additional lithium hydride. Shot 3 is the same as shot 2A, but with a 0.16-cm steel plate in front of the lithium hydride. The axial peak pressure decay curves for both shots are shown in Fig. 11. As can be seen, the effect of the frontal steel plate in shot 3 becomes damped out at large distances from impact. Pressure versus axial distance from impact plots for shot 2A are shown for four selected times after impact in Fig. 12. In addition, relative densities for shot 2A at four

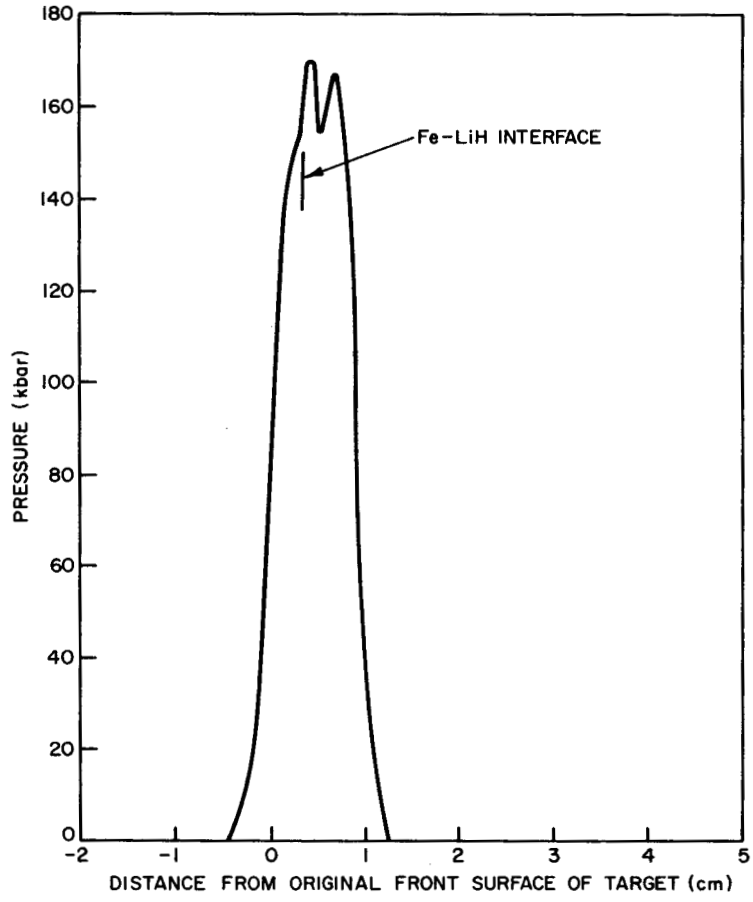

Fig. 6 — Pressure on axis vs distance into target for shot 2 at time 0.88 μsec after impact

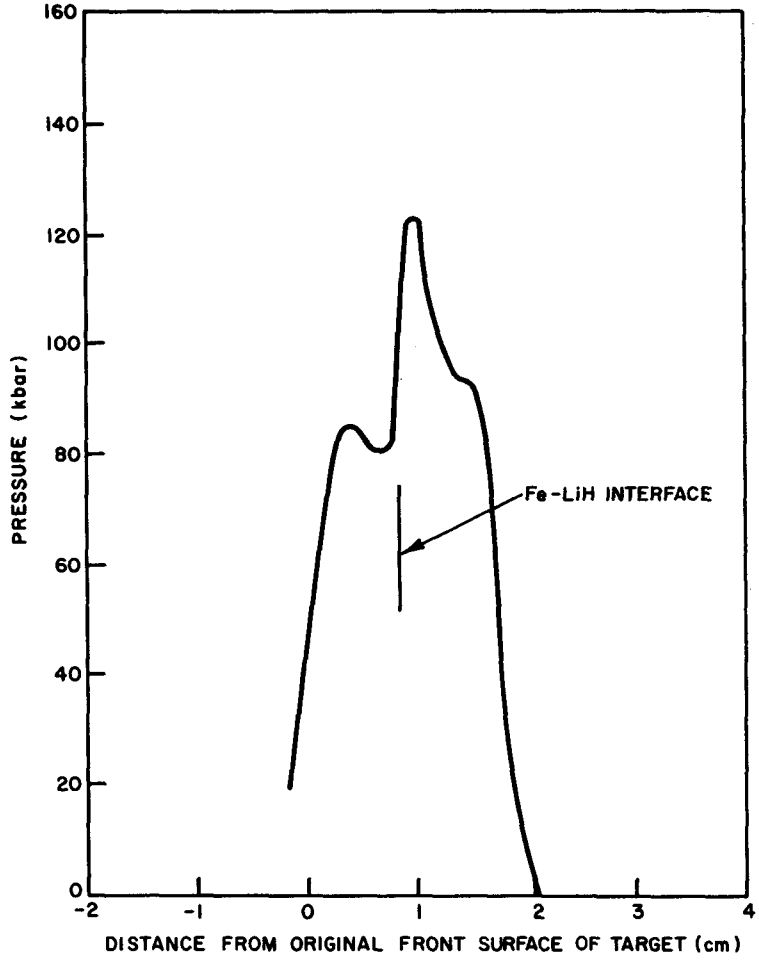

Fig. 7 — Pressure on axis vs distance into target for shot 2 at time 1.82 μsec after impact

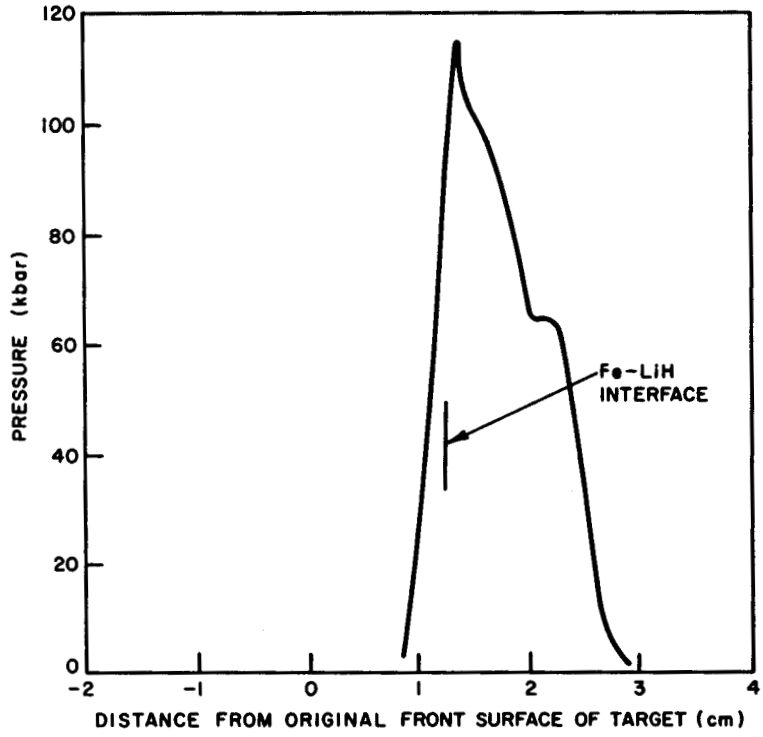

Fig. 8 — Pressure on axis vs distance into target for shot 2 at time 2.76 μsec after impact

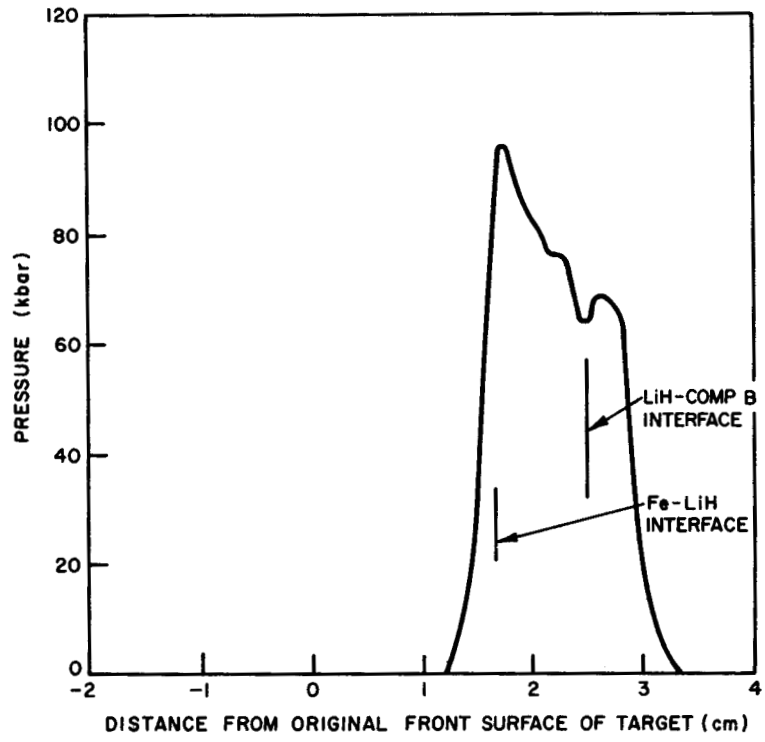

Fig. 9 — Pressure on axis vs distance into target for shot 2 at time 3.74 μsec after impact

selected times are presented in Fig. 13. The method of display is to plot within a cell a number of randomly scattered particles proportional to the relative density in that cell. These particles are *not* carried as part of the calculation, as are the massless "tracer particles," but are created as a means of displaying data only.

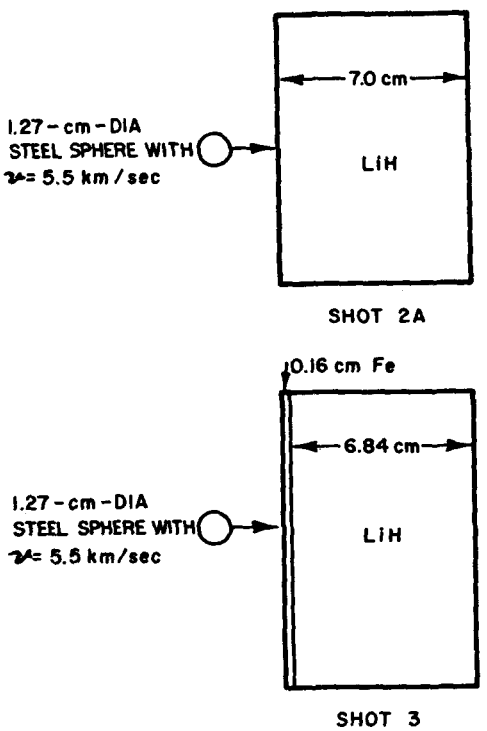

Fig. 10 — Impact configurations for shots 2A and 3

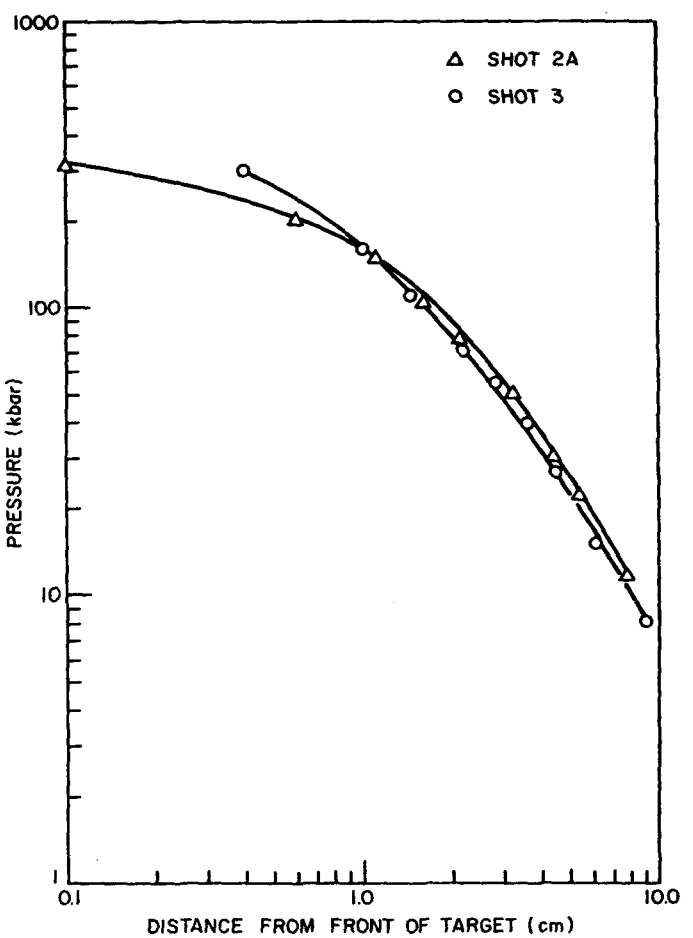

Fig. 11 — Peak shock wave pressure attenuation curves for shots 2A and 3

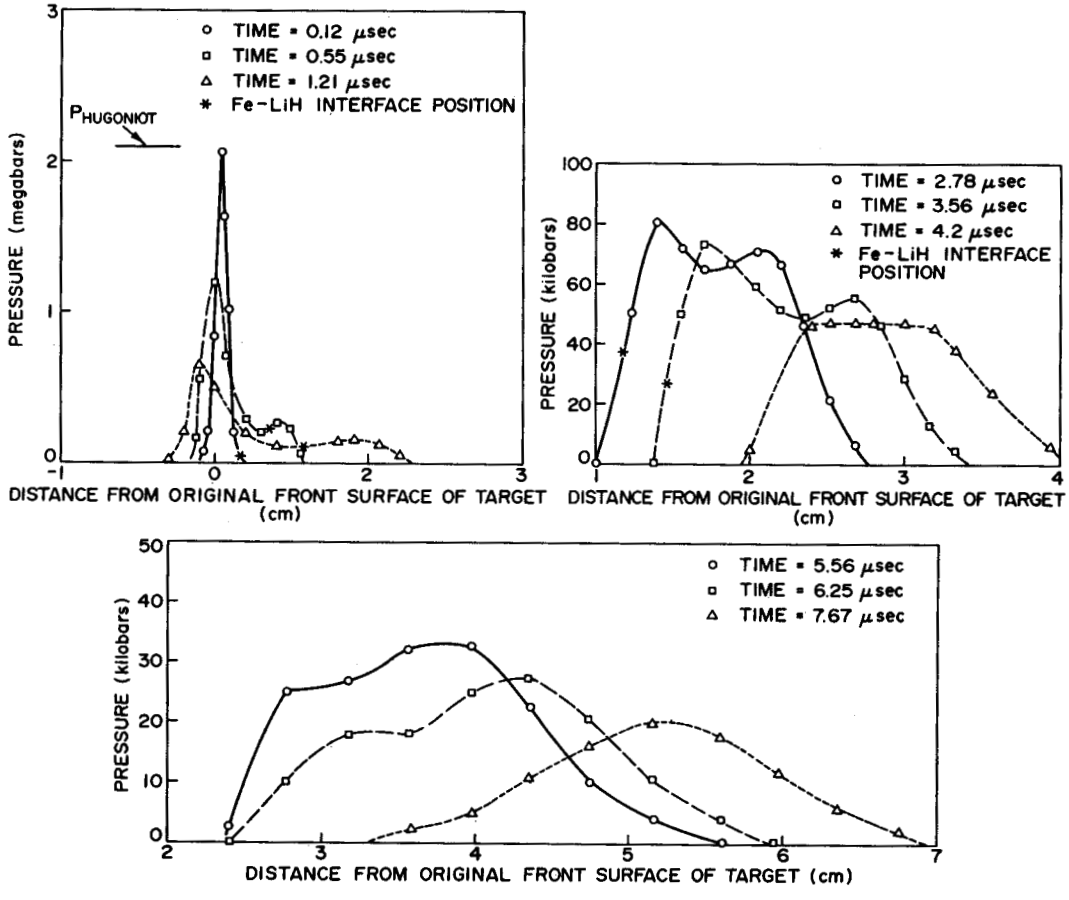

Fig. 12 — Pressure vs distance along axis for shot 2A

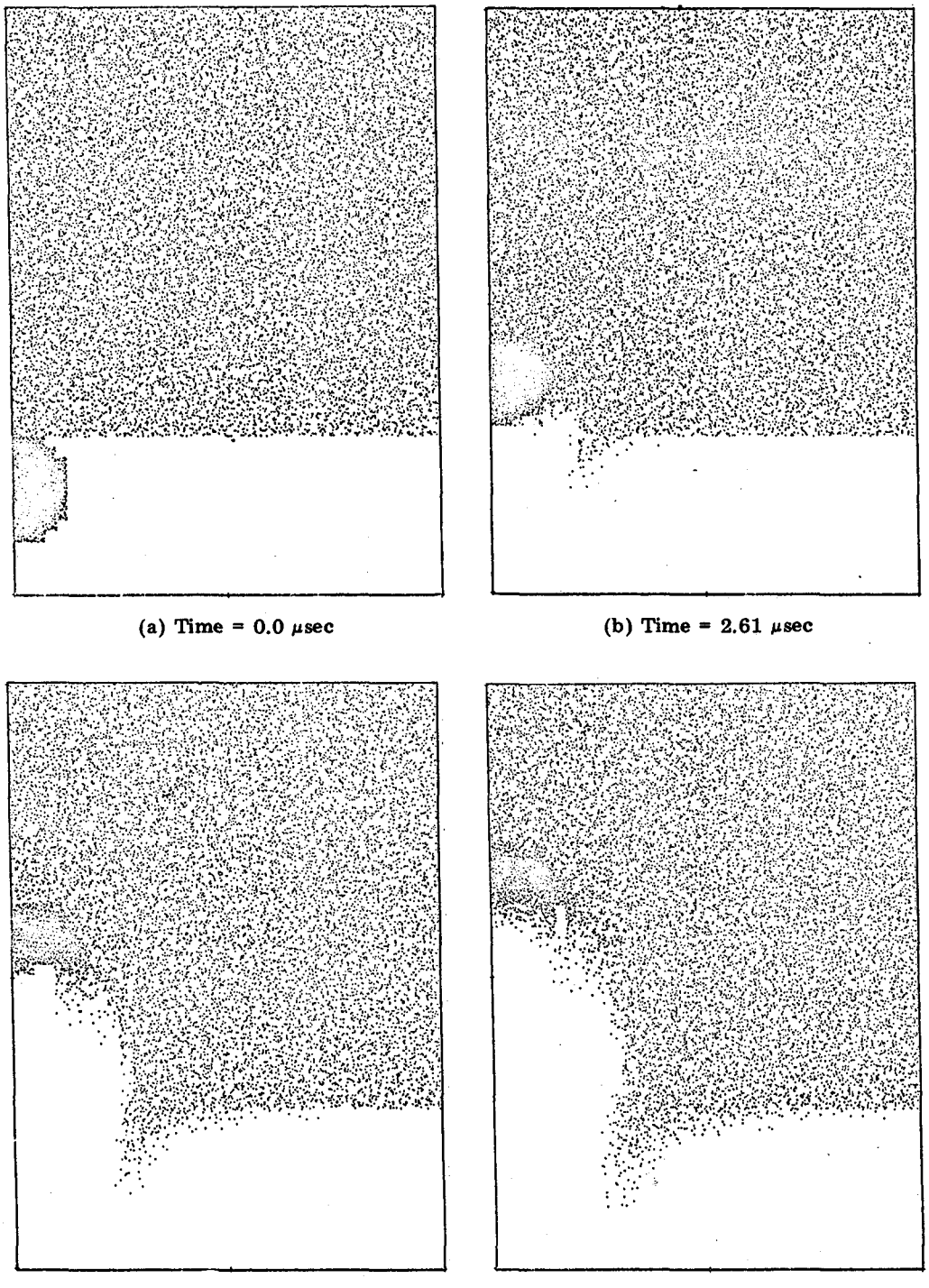

(a) Time = 0.0 μsec

(b) Time = 2.61 μsec

(c) Time = 5.61 μsec

(d) Time = 7.46 μsec

Fig. 13 — Weighted density plots for shot 2A at various times after impact

Single-Plate Rod Impact Calculations (DORF)

The impact of end-oriented metal rods into relatively thin metal plates has been extensively studied, with particular interest attached to the length and velocity loss of the rods after penetration of the plate. Sets of analytical equations for these quantities have been developed which agree quite closely with experimental results. Using the DORF code, seven rod impact calculations were made using single-plate targets to determine the accuracy with which the code could predict rod length loss and residual velocity. The basic configuration and zoning of the problems and tracer particle plots of the impact process are presented in Figs. 14 and 15. The equation-of-state constants used in the calculations are shown in Table 2 and the numerical results in Table 3. The results are quite good, with rod-length-loss calculations differing by no more than about 6% from the experimental values. The residual velocity comparison fares even better, but it should be kept in mind that both the calculated and experimental velocity losses are extremely small. Hence, the residual velocities differ little from the original impact velocities.

The DORF calculations made for this study provided the answer to a question that has been a subject of discussion for quite some time. The analytical approach used in the development of the equations for rod length loss has as one of its hypotheses that the extra length loss over and above that which would be expected from steady-state incompressible flow theory was caused by the initial shock and rarefaction of impact shattering the frontal portion of the rod. However, the experiments of Christman and Gehring (8), where rods were actually x-rayed as they penetrated thick targets, indicate that this is not the case. Also, other projectile configuration experiments at NRL indicate that the extra rod length loss is not a shock-rarefaction phenomenon. To resolve this question, the results of the DORF calculation for an aluminum rod into an aluminum plate with a rod diameter of 1 cm, a plate thickness of 4 cm, and an impact velocity of 4.6 km/sec are plotted in Fig. 16. The solid line shows the rod length loss as a function of rod front position that would be predicted by steady-state incompressible flow theory. The DORF data points do not deviate significantly from this line until the rod front is past the original back of the plate, indicating that the extra rod loss is *not* a shock-rarefaction phenomenon, but is associated with the breakout of the rod from the back of the target.

Low-Velocity Multimaterial Impact (DORF9)

Two important features of the DORF9 code for impact calculation purposes are its ability to treat up to nine different materials in a problem and its ability to treat material strength (using a rigid plastic model). Both of these features were tested by calculating the low-velocity (3.048 km/sec) impact of a steel cylinder into an ablative layer backed up with aluminum. The impact configuration is shown in Fig. 17. The equation-of-state constants used in the calculation are listed in Table 2. The results are highly strength dependent, since the projectile will be deformed and decelerated by the impact, but will do very little actual flowing. Figure 18 compares the calculated projectile configuration after impact, using a tracer-particle plot and an actual photograph of the projectile after impact. The similarity is very close. Calculated residual length is 70% versus 68% experimental. Calculated residual velocity is 2.54 km/sec; the experimentally measured value is 2.60 km/sec.

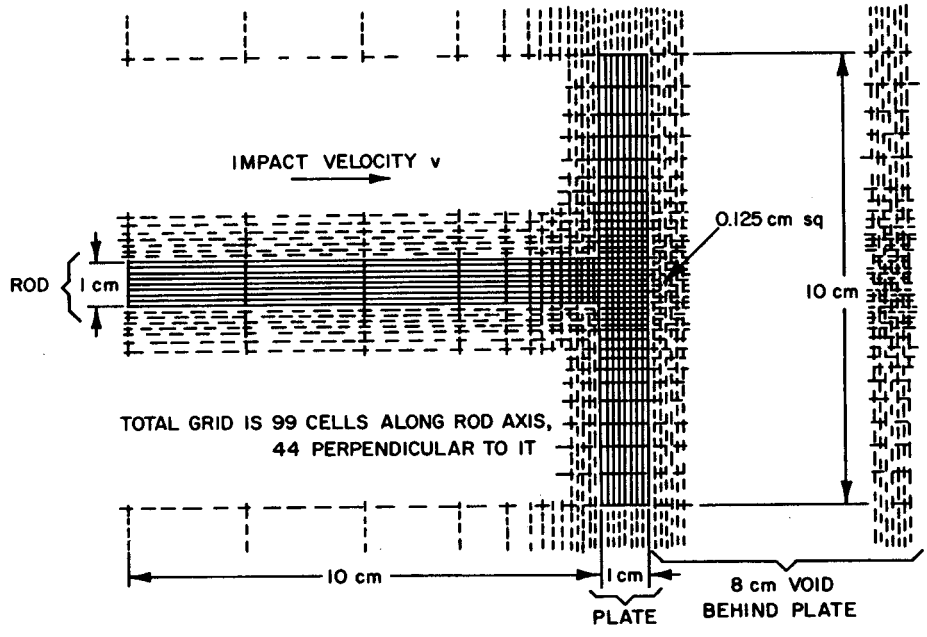

Fig. 14 — Basic configuration and zoning of single-plate rod impact calculations. The thicker and thinner target calculations were made by filling in or deleting material in the void behind the plate.

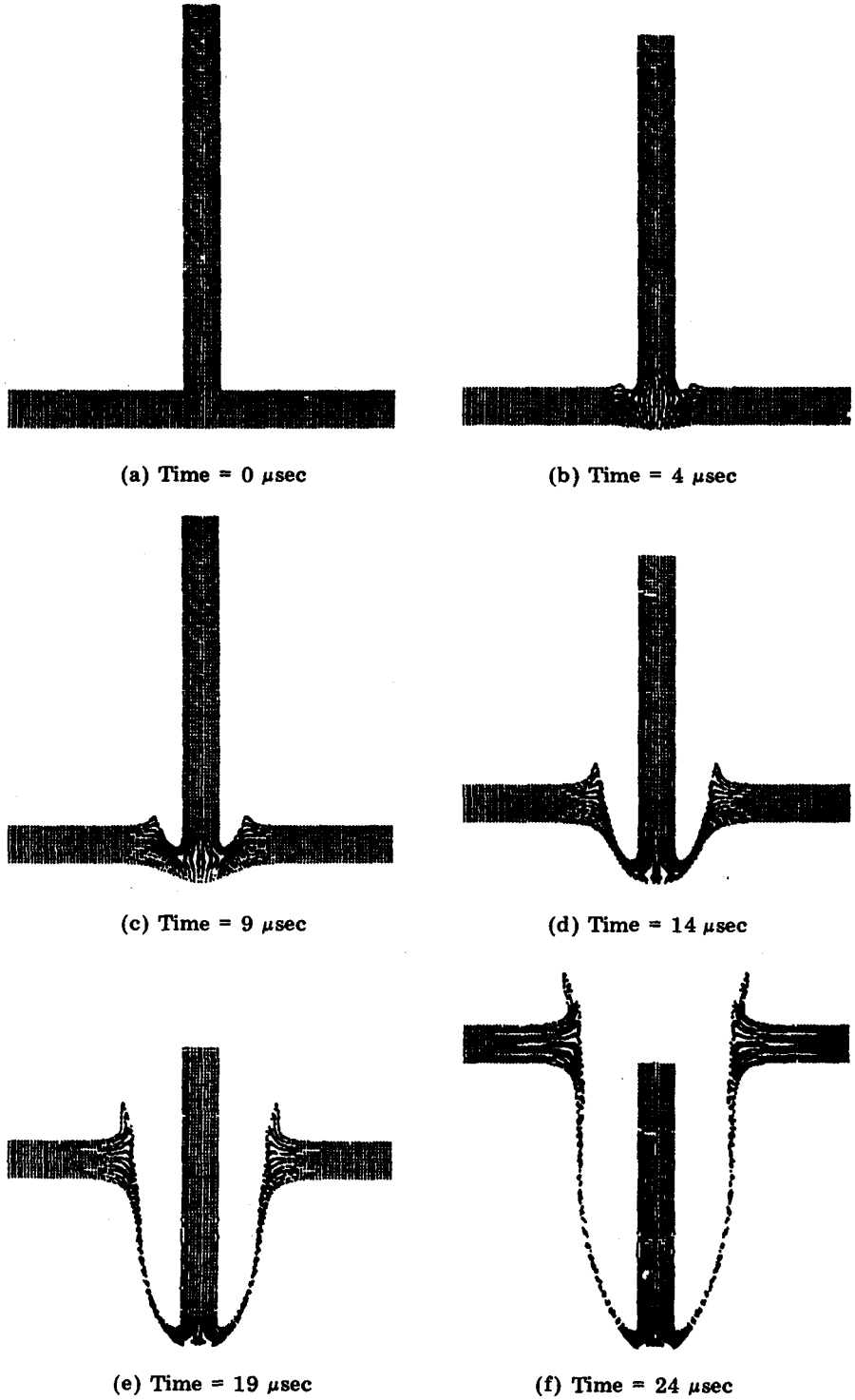

Fig. 15 — Tracer particle plots at selected times after impact for a 1.0-cm-diameter aluminum rod 10 cm long impacting a 1-cm-thick aluminum plate at 4.6 km/sec

Table 2
Tillotson Equation-of-State Constants for Various Materials

Variable	Al	Fe	LiH	Composition B	Astrolite
ρ (g/cc)	2.7	7.86	0.78	1.715	1.7
a	0.5	0.5	0.8	0.8	0.6
E_0 (jerks/g)	5.0×10^{-6}	9.5×10^{-6}	1.0×10^{20}	1.0×10^{20}	7.0×10^{-6}
b	1.63	1.5	0.	0.	2.0
A (jerks/cc)	7.52×10^{-5}	1.279×10^{-4}	3.5×10^{-5}	2.08×10^{-5}	2.455×10^{-5}
E_s (jerks/g)	3.0×10^{-6}	2.44×10^{-6}	2.0×10^{-5}	2.0×10^{-6}	2.4×10^{-6}
E_s' (jerks/g)	1.5×10^{-5}	1.02×10^{-5}	3.0×10^{-5}	1.8×10^{-5}	1.8×10^{-5}
α	5.0	5.0	5.0	5.0	10.0
β	5.0	5.0	5.0	5.0	5.0
B (jerks/cc)	6.5×10^{-5}	1.05×10^{-4}	3.5×10^{-5}	2.08×10^{-5}	6.55×10^{-6}
C_0 (10^5 cm/sec)	5.28	5.13	6.3	2.75	2.86
ξ_1	4.4	3.4	6.0	2.75	8.3
ξ_2	0.45	0.42	0.5	0.5	0.45
E_m (jerks/g)	1.01×10^{-6}	9.16×10^{-7}	2.0×10^{-5}	2.0×10^{-6}	8.0×10^{-7}
α'	0.07	0.07	0.07	0.07	0.5
Y_0 (jerks/cc)	3.4×10^{-7}	6.8×10^{-7}	4.0×10^{-8}	1.0×10^{-9}	1.0×10^{-7}

NOTE: 1 jerk = 10^{16} ergs, 1 shake = 10^{-8} sec, and 10^{-7} jerks/cc = 1 kilobar.

Table 3
Single-Plate Rod Impacts
DORF Code Calculations vs Experiment

Projectile Material	Target Material	Velocity (km/sec)	Plate Thickness	Length Loss ($\Delta\ell/d$)		Residual Velocity (km/sec)	
			(t/d)	DORF	Experiment	DORF	Experiment
Al	Al	4.6	1/2	1.84	1.78	4.588	4.554
Al	Al	4.6	1	2.49	2.54	4.555	4.550
Al	Al	4.6	2	3.87	3.72	4.554	4.540
Al	Al	4.6	4	6.12	6.15	4.466	4.504
Al	Al	6.1	1	2.66	2.56	6.053	6.050
Al	Steel	4.6	1	4.10	4.38	4.569	4.533
Steel	Steel	4.6	1	2.56	2.45	4.567	4.543

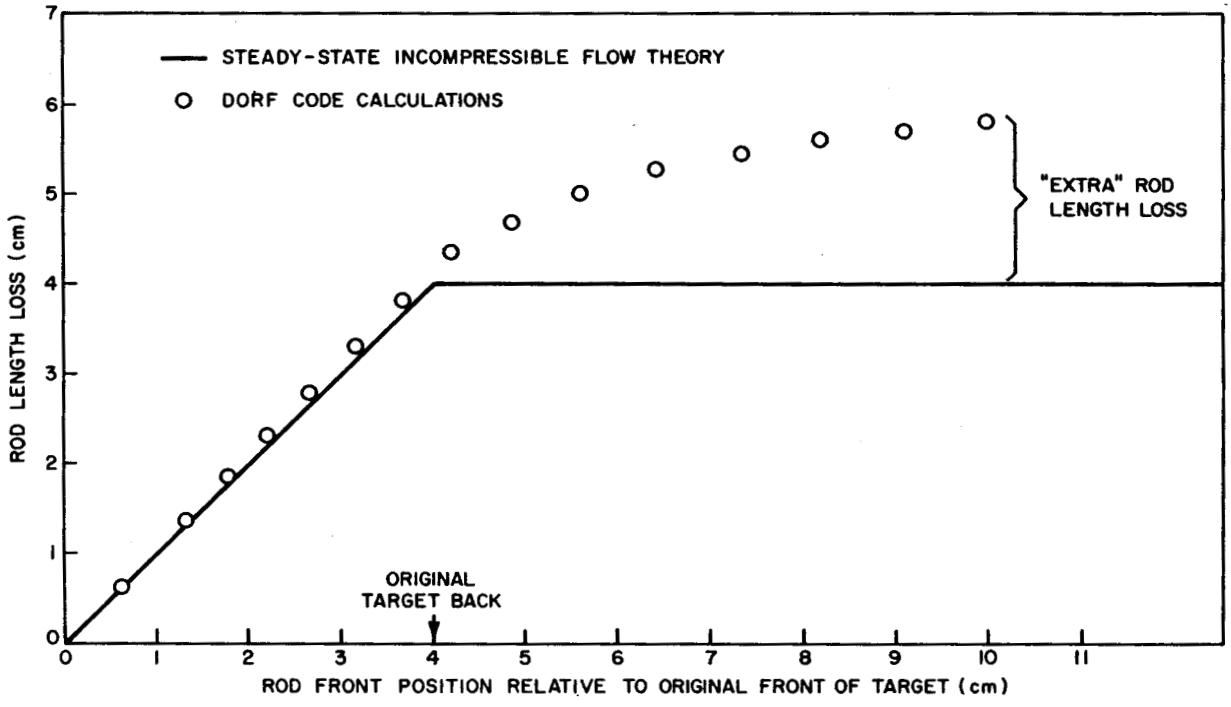

Fig. 16 — Rod length loss vs rod front position in target for 1-cm-diameter 10 cm long aluminum rod impacting a 4-cm-thick aluminum plate at 4.6 km/sec

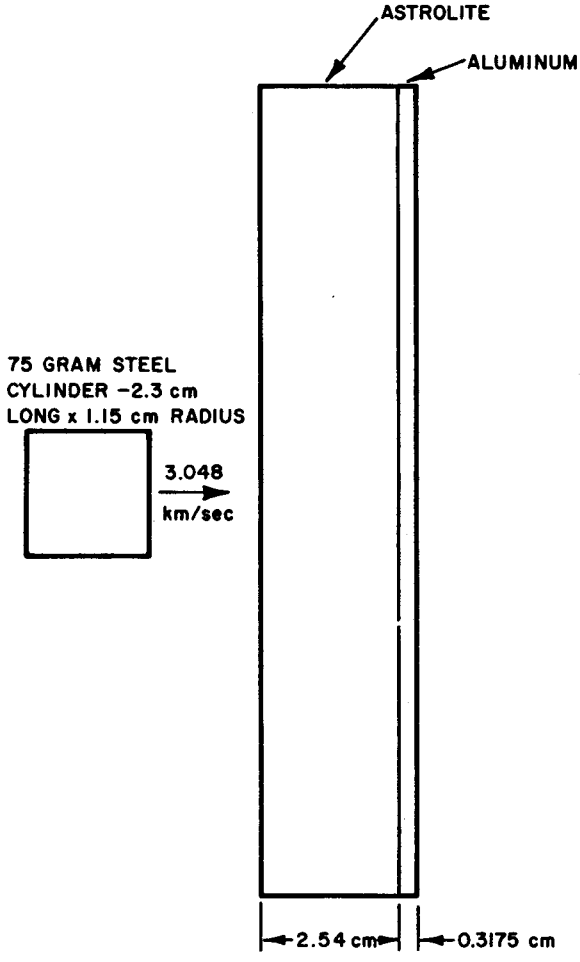

Fig. 17 — Impact configuration for low-velocity impact

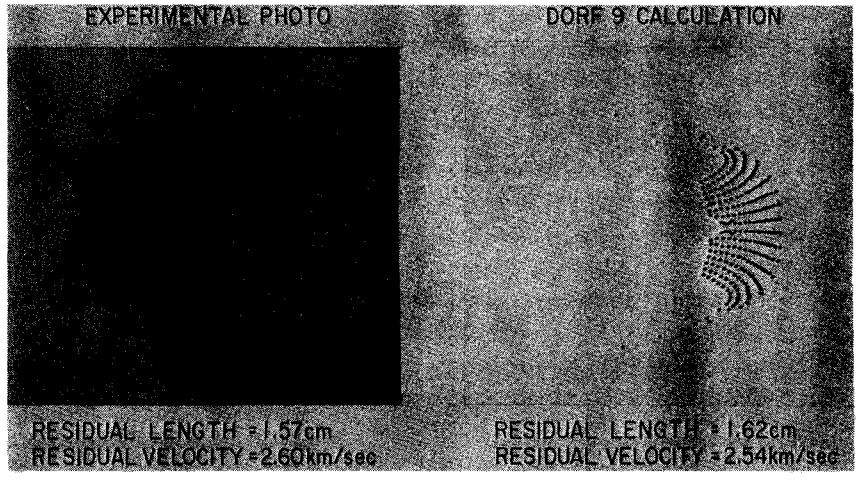

Fig. 18 — Residual projectile after low-velocity impact DORF9 code calculations vs experiment

CONCLUSIONS

The experiment-code comparisons that have been presented here obviously reflect very favorably on the ability of the codes to predict reality. It should be pointed out, however, that only certain specialized phenomena were considered in this study: shock-wave pressure attenuation, projectile length loss, deformation and velocity loss, and total target penetration. Lateral damage to the target was not considered (the problems were zoned finely only near the projectile trajectory axis, leaving coarse zoning in those regions off the axis where one might expect the lateral damage to be defined). However, good correlation for lateral damage to cadmium plates impacted by cadmium spheres, as well as for pressure distribution on a second plate, has previously been reported by one of the authors (9). It is felt that the codes are extremely useful tools for hypervelocity impact problems, as long as care and an understanding of their weakness are exercised. It is highly probable that other fields of endeavor could benefit from their utilization.

REFERENCES

1. W. E. Johnson, "Development and Application of Computer Programs related to Hypervelocity Impact," 3SR-353, Annual Report, December 1970, Systems, Science, and Software Sponsored by Advanced Research Projects Agency, ARPA Order 854.
2. W. E. Johnson, "Development and Application of Computer Programs related to Hypervelocity Impact," 3SR-749, Annual Report, July 1971, Systems, Science, and Software, Sponsored by Advanced Research Projects Agency, ARPA Order 854.
3. J. H. Tillotson, "Metallic Equations of State for Hypervelocity Impact," General Atomics Report GA-3216, July 1962.
4. J. R. Baker, and S. T. Zalesak, "Manganin Gauge Measurements of Shock Wave Profiles for Impact of a Spherical Projectile," Proceedings of the 18th Meeting of the Aeroballistic Range Association, Vol. 1.
5. J. A. Charest, "Measurements of Shock Wave Pressures Generated by Hypervelocity Impacts in Aluminum," General Motors Corporation Report TR-64-58 Nov. 1964, sponsored by NASA/Marshall Space Flight Center.
6. M. H. Rice, R. G. McQueen, and J. M. Walsh, "Compression of Solids by Strong Shock Waves," Solid State Physics, Vol. 6, Academic Press, New York, 1958, p. 1.
7. L. V. Al'tshuler, S. B. Kormer, A. A. Bakanova, and R. F. Trunin, J. Expt 1. Theoretical Physics, (U.S.S.R.) 38, 790-798, (1960); Soviet Phys. JETP 11, 573-579 (1960).
8. D. R. Christman and J. W. Gehring, "Analysis of High-Velocity Projectile Penetration Mechanics," J. Appl. Phys. 37, No. 4, 1579-1587 (1966).
9. W. E. Johnson, "Code Correlation Study," Technical Report, AFWL-TR-70-144, Apr. 1971.

Appendix A

SIMPLIFIED FLOW CHART FOR DORF9

START

READ THE DUMP TAPE FOR THE CORRECT CYCLE NUMBER.

RECYCLE

CDT

CALCULATE THE HYDROSTATIC PRESSURE FROM THE EQUATION OF STATE AND THE TIME STEP (Δt) FROM BOTH THE COURANT CONDITION AND THE PARTICLE VELOCITIES.

EDIT

CALCULATE INTEGRAL QUANTITIES, PRINT CELL QUANTITIES, DUMP VARIABLES FOR RESTART OR FOR PLOTTING.

PH1

THE EQUATIONS OF CONSERVATION OF MOMENTUM AND ENERGY (DUE TO PRESSURE FORCES ONLY) ARE SOLVED. SINCE NO MASS IS MOVED AT THIS STAGE OF THE CALCULATION, PHASE 1 IS IDENTICAL TO A LAGRANGIAN CALCULATION. NOTE THAT THE TRANSPORT TERMS ARE TEMPORARILY DROPPED.

CONSERVATION OF MOMENTUM:

$$\rho \frac{\partial \mathbf{u}}{\partial t} = -\nabla P$$

CONSERVATION OF ENERGY:

$$\rho \frac{\partial I}{\partial t} = -P \nabla \cdot \mathbf{u}$$

PH3

HERE THE DEVIATORIC STRESSES (RIGID PERFECTLY PLASTIC) ARE COMPUTED AND THEIR CONTRIBUTIONS TO THE VELOCITIES AND ENERGY ARE ACCOUNTED FOR. THESE DEVIATOR STRESSES σ ARE FUNCTIONS ONLY OF VELOCITY GRADIENTS, WHERE THE VELOCITIES TO BE USED ARE THOSE FROM PHASE 1. IN TENSOR NOTATION THE EQUATIONS, AGAIN DROPPING TRANSPORT TERMS, ARE:

CONSERVATION OF MOMENTUM:

$$\rho \frac{\partial u_i}{\partial t} = + \sigma_{ij,j}$$

CONSERVATION OF ENERGY:

$$\rho \frac{\partial E}{\partial t} = (\sigma_{ij} u_i)_{,j}$$

HERE E IS THE TOTAL ENERGY PER GRAM, INTERNAL PLUS KINETIC.

PH2

FINALLY, THE TRANSPORT TERMS, THAT WERE TEMPORARILY OMITTED IN PHASE 1 AND PHASE 3 ARE SOLVED FOR, AND THE MASSES, VELOCITIES, AND SPECIFIC INTERNAL ENERGIES ARE INTEGRATED TO TIME $t + \Delta t$.

CONSERVATION OF MASS:

$$\frac{\partial \rho}{\partial t} + \nabla \cdot \rho \mathbf{u} = 0$$

CONSERVATION OF MOMENTUM:

$$\frac{\partial \rho \mathbf{u}}{\partial t} = -\nabla \cdot (\rho \mathbf{u}\mathbf{u})$$

CONSERVATION OF ENERGY:

$$\frac{\partial \rho E}{\partial t} = -\nabla \cdot \rho \mathbf{u} E$$

RECYCLE

Unclassified

Security Classification

DOCUMENT CONTROL DATA - R & D

(Security classification of title, body of abstract and indexing annotation must be entered when the overall report is classified)

1. ORIGINATING ACTIVITY *(Corporate author)* Naval Research Laboratory Washington, D.C. 20390	2a. REPORT SECURITY CLASSIFICATION 2b. GROUP 3

3. REPORT TITLE

THEORETICAL AND EXPERIMENTAL IMPACT STUDIES [Unclassified Title]

4. DESCRIPTIVE NOTES *(Type of report and inclusive dates)*

A final report on this phase of the problem; work is continuing on other phases.

5. AUTHOR(S) *(First name, middle initial, last name)*

W. E. Johnson and S. T. Zalesak

6. REPORT DATE November 3, 1972	7a. TOTAL NO. OF PAGES 30	7b. NO. OF REFS 9
8a. CONTRACT OR GRANT NO. NRL Problem F04-21 b. PROJECT NO. ARPA Order 854 c. N00014-70-C-0002 d.	9a. ORIGINATOR'S REPORT NUMBER(S) NRL Report 7398 9b. OTHER REPORT NO(S) *(Any other numbers that may be assigned this report)*	

10. DISTRIBUTION STATEMENT

11. SUPPLEMENTARY NOTES	12. SPONSORING MILITARY ACTIVITY Advanced Research Projects Agency, Arlington, Virginia 22209

13. ABSTRACT [Unclassified]

Thin, layered, and semi-infinite targets have been impacted experimentally, and theoretical calculations performed by the DORF code for these same target impacts. The DORF code is a two-material, two-dimensional continuous Eulerian hydrodynamic code coupled with a rigid, perfectly plastic strength model. In addition, DORF9, a nine-material version of DORF, has calculated several of the impact experiments. The agreement is good between the theoretical calculations and experimental values for shock attenuation and projectile length loss.

DD FORM 1 NOV 65 1473 (PAGE 1)

S/N 0101-807-6801

Unclassified

Security Classification

Unclassified

Security Classification

14. KEY WORDS	LINK A ROLE	LINK A WT	LINK B ROLE	LINK B WT	LINK C ROLE	LINK C WT
Hypervelocity impact						
Hydrodynamic computer codes						
DORF code						

DD FORM 1 NOV 65 1473 (BACK)

(PAGE 2)

Unclassified

Security Classification